Coarse-grained molecular-dynamics simulations of capped crosslinked polymer films

Coarse-grained molecular-dynamics simulations of capped crosslinked polymer films: equilibrium structure and glass-transition temperature

T. Davris[1] and A.V. Lyulin[1]

[1]Theory of Polymers and Soft Matter, Technische Universiteit Eindhoven, P.O. Box 513, 5600 MB Eindhoven, the Netherlands

Coarse-grained molecular-dynamics simulations of capped crosslinked polymer films: equilibrium structure and glass-transition temperature

T. Davris[1] and A.V. Lyulin[1]

[1]Theory of Polymers and Soft Matter, Technische Universiteit Eindhoven, P.O. Box 513, 5600 MB Eindhoven, the Netherlands

We present our recent results from constant temperature-pressure (NPT) molecular dynamics (MD) simulations of a bead-spring copolymer model, in which the polymer is confined between two crystalline substrates. Our goal was to study the combined effect of the polymer crosslinking density and the degree of confinement on the glass-transition temperature and the equilibrium structure of the films. In the direction perpendicular to the substrates, the polymer chains are ordered in layers of increasing density towards the substrates, for all crosslinking densities and the degrees of confinement. In the direction parallel to the substrates, the polymer films display an amorphous structure, just like in the bulk. The glass-transition temperature increases with confinement and crosslinking density, with the former having a large effect compared to the later.

INTRODUCTION

Filled elastomers, realized by mixing pure rubber with filler particles of sub-micron or nanometer size, are a class of materials of high technological importance, being used in car tires, sealing solutions for bearing applications and other types of plastic and rubber. The addition of particles to the polymer matrix results in a composite material that exhibits much higher stiffness and extreme resistance to both fracture and abrasion while remaining highly elastic (the so-called reinforcement of rubber) [1]. At a fundamental level, rubber-reinforcement is a complex function of interfacial interactions, interfacial area and the distribution of inter-filler distances [1,2]. The latter two factors depend on nano-filler dispersion, making it difficult to develop a fundamental understanding of their effects on nanocomposite properties.

Various attempts to study the influence of confinement on the mechanical properties of polymer nanocomposites have deployed a film polymer model, where the authors have tried to establish a quantitative equivalence between the thermo-mechanical properties of the two systems [2-5]. The main argument is that the properties of both systems are strongly influenced by the polymer-surface interactions and confinement effects, and that a connection exists in cases where the average diameter of the filler particles is orders of magnitude larger than the size of the chains.

Bansal et al. [2] have shown that the experimental thermo-mechanical properties of highly filled (40 wt%) polymer nanocomposites are quantitatively equivalent to the well documented case of planar polymer films. They quantified this equivalence by drawing a direct analogy between film thickness and inter-particle spacing. They showed that the changes in the glass-transition temperature (T_g) with decreasing the inter-particle spacing for two filler surfaces are quantitatively equivalent to the corresponding thin film data.

Similar experiments with materials of a lower filler concentration (less than 1.0 wt%) showed only a qualitative equivalence between nanocomposites and thin films [2,5]. Kropka and coworkers examined the changes in the T_g for polymer nanocomposites and their equivalence to thin films in terms of a percolation model. While the qualitative behavior of both systems was similar, clear quantitative differences were discerned. However, a phenomenological model was suggested that could use results from thin film simulations to predict quantitatively the properties of polymer nanocomposites.

A variety of simulations, employing either a film or a nanocomposite model, are reported in the literature that were directed to the study of the structural, dynamical, and mechanical properties of polymer nanocomposites [12, 6, 7-11]. Khare et al. [C] used atomistic molecular simulations to study the effect of nanofiller dispersion on the T_g of carbon nanotube (CNT) nanocomposites within a crosslinked epoxy matrix. They asserted that the polymer-filler interactions were unfavorable, to explain the observed depression in the T_g compared to the neat polymer matrix. Batistakis and coworkers [7,8,12] studied the confinement-induced creation of glassy layers employing a similar to ours, though non-crosslinked, polymer film model. In their simulations, the chosen statistical ensemble had an important effect on the T_g dependence on the film thickness. Their *NPT* simulations resulted in an increasing T_g when the degree of confinement and the polymer-substrate attraction strength were independently increased, whereas the opposite dependence was observed under *NVT* conditions upon changing the film thickness. Guseva et al. [10] carried out atomistic *NPT* molecular-dynamics simulations of a non-crosslinked (1,4) cis-polyisoprene melt confined between two amorphous, fully coordinated silica surfaces. They reported a profound increase of the T_g in strongly confined systems, whereas no effect of confinement was observed in thicker films. In this paper we aim to extend these studies by modeling the structural changes that are induced by the combination of confinement effects and the polymer crosslinking density in

caped polymer films. In general, a variety of polymer films simulations have shown that the relaxation dynamics depend on the nature of the substrate [13]. Strongly attractive substrates may slow down relaxation [16,17], weakly attractive substrates have a very small effect [16], whereas repulsive substrates or free surfaces result in accelerated relaxation [14-15, 18].

A number of simulation data is present in the literature concerning the effect of crosslinking on the structural, dynamical, and mechanical properties of polymer systems [19-23]. Liu et al [19] performed molecular dynamics (MD) simulations to study the effect of the crosslinking density on the structural and dynamic properties of a bead-spring bulk homopolymer system. They observed that the radial distribution function of the monomer segments was not affected by the presence of crosslinks. On the other hand, the glass-transition temperature displayed a positive linear variation with the crosslinking density, while the self-diffusion coefficient displayed a stronger (exponential) negative dependence.

The glass transition in thin polymer films has also been widely examined using different experimental techniques [24-32]. The reported results, concerning the direction of the glass-transition change upon changing the degree of confinement, have shown disagreement among different experimental methods and different laboratories. The generally accepted opinion is that the behavior of T_g in films depends on the degree of confinement, the presence of free interfaces, the film preparation method, the film annealing, as well as many other details. The effect of the polymer-substrate interactions is especially important when the thickness of the film becomes smaller than a specified length scale [23, 32]; a depression in the T_g is generally observed for unfavorable or weak interactions, whereas an increasing T_g is observed in the case of attractive interactions. Concerning the influence of the adhesion interactions, a number of experimental and simulation studies [10, 33-35] on supported or free-standing films have reported a T_g shift of 10-50K upon changing the polymer-substrate interaction strength. Putz et al. [36] studied the impact of the crosslinking density on the T_g, by

conducting DSC (dynamic scanning calorimetry) experiments on an epoxy polymer nanocomposite. The results indicated an increased T_g for low values of the crosslinking density and a decreased T_g for higher values, in comparison to the bulk polymer.

In this paper we study how the structural properties and the glass-transition temperature of the polymer are influenced when it is crosslinked and confined between two substrates. Besides identifying the glass transition using only a single number (T_g), we have also determined the differences in thermal expansivities between the rubbery and glassy states.

MODELS AND METHODS

Model Description

We performed molecular-dynamics simulations of polymer chains confined between two crystalline substrates using the LAMMPS software package [37]. We used a coarse-grained representation of a polymer film consisting of 100 linear copolymer chains with a fixed size of 50 monomer segments per chain [38]. Eighty percent of the monomers of each chain are of type A, and we denote the rest as type B monomers. We use the letter S to denote the substrate segments, all of which are of the same type. Moreover, we compared the film data with results produced by simulations performed in the bulk. Note also that we regard the polymer chains as non-entangled. This is because all the microscopic topological constraints we identified were short-lived and thus unable to sustain stress [39].

We placed the system in a three-dimensional periodic box. Each substrate was composed of three lateral layers of equally sized non-bonded beads arranged in a hexagonal closed packed (HCP) regular lattice. They are periodically infinite along the lateral dimensions, and they confine the polymer along the perpendicular direction, as depicted in Fig. 1. When we chose the thickness of the substrates we made sure not to violate the minimum image criterion, also taking into account their periodic image along the perpendicular direction.

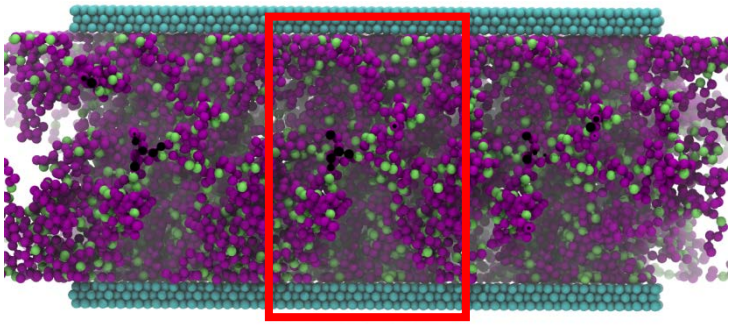

FIG 1: A snapshot of the simulated copolymer that is confined between two crystalline substrates. Different colors are used to represent different bead types. The red rectangle depicts the periodic simulation box. We created the illustration using the molecular visualization software VMD [40].

The non-bonded interactions were modelled with the Lennard-Jones (LJ) 12-6 potential, including a switching function $S_{f(r)}$, that ramps the energy and force smoothly to zero between $r_{\text{cut}}^{\text{in}} = 3.25\sigma$ and $r_{\text{cut}}^{\text{out}} = 3.50\sigma$ [41].

$$U_{\text{ST}}(r) = 4\varepsilon\left[\left(\frac{\sigma}{r}\right)^{12} - \left(\frac{\sigma}{r}\right)^{6}\right] + S_{f(r)} \quad (r < r_{\text{cut}}^{\text{out}}) \tag{1}$$

The Lenard-Jones (LJ) units of measurements have been used throughout the paper, i.e. m is the unit of mass, ε is the unit of energy, σ is the unit of length and τ is the unit of time, where $\tau = \sigma\sqrt{m/\varepsilon}$. We have chosen the following values for the LJ parameters: $\sigma_{\text{AA}} = \sigma$, $\varepsilon_{\text{AA}} = \varepsilon$, $m_{\text{A}} = m$, $\sigma_{\text{BB}} = 1.2\sigma$, $m_{\text{B}} = (\sigma_{\text{B}})^3 m$, $\varepsilon_{\text{BB}} = \varepsilon$, $\sigma_{\text{SS}} = 0.85\sigma$, and $\varepsilon_{\text{SS}} >> \varepsilon$. The LJ parameters between beads of different types were calculated according to Lorentz-Berthelot rule, $\sigma_{\text{ij}} = (\sigma_{\text{ii}} + \sigma_{\text{jj}})/2$, but the energies were fixed, i.e., $\varepsilon_{\text{AB}} = \varepsilon_{\text{AS}} = \varepsilon_{\text{BS}} = \varepsilon$. The interaction strength between substrate beads, ε_{SS}, was chosen high enough to ensure that the crystallinity

of the substrates was never broken. The size of the substrate beads, $\sigma_{SS,}$ was chosen smaller than the smallest monomer type to avoid the adsorption of monomers on the internal surface of the substrates due to geometric constraints [7]. We did not account for electrostatic Coulomb interactions or for long-range energy corrections.

Covalently bonded beads interact through a combination of an attractive Finite-Extensible-Nonlinear-Elastic (FENE) potential and a repulsive and truncated LJ 12-6 potential [42].

$$U_{\mathrm{FENE}}(r) = -0.5\, k_{\mathrm{FENE}}\, R_{\mathrm{max}}^2\, \ln\left[1 - \left(\frac{r}{R_{\mathrm{max}}}\right)^2\right] + 4\varepsilon\left[\left(\frac{\sigma}{r}\right)^{12} - \left(\frac{\sigma}{r}\right)^{6}\right] + \varepsilon \qquad (2)$$

The parameters k_{FENE} and R_{max} are the stiffness and maximum elongation of the spring, respectively, ε is the LJ energy parameter, and σ is the collision diameter of the interacting beads. The stiffness and maximum elongation of the bonded potential were set equal to $k_{\mathrm{FENE}} = 30\varepsilon/\sigma^2$ and $R_{\mathrm{max}} = 1.5\sigma$, respectively. The LJ parameters ε and σ have the same values with their non-bonded counterparts. This particular choice of bonded and non-bonded interactions prevents chain crossings [38] and crystallization [42-44]. An additional consequence of this model is that chains do not become stiffer with decreasing temperature. Newton's equations of motion were integrated by the velocity Verlet algorithm using a time step of $\delta t = 0.001\tau$.

System Preparation and Equilibration

The initial dimensions of the simulation box were calculated according to the chosen polymer mass density of $\rho_{\mathrm{film}} = 1.0\, m/\sigma^3$. We studied three films of different thickness, i.e., at $T = 1.5\ \varepsilon/k_B$, the thickness of the films were $D = 22.5\sigma$ (thick film), $D = 12.0\sigma$ (thin film), and $D = 5.1\sigma$ (ultrathin film), which corresponded approximately to 6.2, 3.3, and 1.4 times the average radius of gyration of the chains in the bulk, respectively. Films of different

thickness had different lateral dimensions, in order for the mass density to be the same. Due to the crystallinity of the substrates, the lateral dimensions of the box were only approximately equal, but in all cases the difference was kept smaller than 0.5σ.

The initial configuration of the chains was created using a simple random walk algorithm. No overlap checking was done, so the initial structures displayed a finite number of overlaps. The crosslinking procedure was based on the equilibrated uncured system. Crosslinks were created between monomers belonging to different chains until the system had reached the desired crosslinking number density

$$\rho_{\mathrm{cl}} = \frac{\text{total number of crosslinks}}{\text{number of chains}} \tag{3}$$

The first step was to refold all chains that were completely outside the periodic box. This was done in order to increase the number of beads whose distance was smaller than the specified crosslinking radius. The next step was to identify all candidate monomer pairs whose distance was smaller than the crosslinking cut-off radius. Crosslink bonds were then created between a randomly chosen candidate pair of monomers until the desired value of the crosslinking number density was reached. Using this method, crosslinked clusters were created with only a small fraction of free (non-crosslinked) chains. The spatial distribution of crosslinks along the direction perpendicular to the substrates was approximately uniform for all systems except for the ultra-thin film where a higher concentration of crosslinks was produced near the substrates rather than in the middle of the film.

For both equilibration and production runs, we used the default LAMMPS values for the applied thermostat and barostat [37]. During the equilibration, the two phases of the system (polymer and substrates) displayed a tendency to move laterally. To prevent this, the center-of-mass linear velocity of the substrate and polymer phases were set individually equal to

zero, at each timestep. In order to minimize the substrate-polymer interactions during the first stages of the equilibration, we set the cut-off radius of their interaction equal to the collision diameter between a substrate and polymer bead (the distance for which the interaction energy is zero). In this way, monomer and substrate beads repelled each other only when they collided.

To diminish the initial overlaps among the monomers, a short MD run was performed, for about 100-500τ in the microcanonical (NVE) ensemble while a limit was imposed on the maximum distance a bead can move in one timestep. After the pressure had stabilized, the substrate and monomer beads were assigned random velocities drawn from a Gaussian distribution. We specified the initial velocities of the monomers so that each sub-system would have an initial high temperature of 1.5 ε/k_B and the equilibration of the system would be accelerated.

Next, we performed constant density-temperature simulations using the Berendsen thermostat, initially with repulsive adhesion interactions for about 30,000τ, depending on the film thickness, and afterwards using the full LJ potential (Eq. 1) for another 30,000τ. The combination of a single thermostat with repulsive adhesion interactions resulted in a considerable amount of heat transfer taking place from the substrates to the polymer, while the average temperature of the whole system remained constant and equal to the target value. To overcome this problem, we used two separate thermostats for substrates and polymer while the substrate-polymer interactions were repulsive. During the final equilibration step, we allowed the system to relax in an unstressed state for about 30,000τ by using the Nose-Hoover thermostat and barostat and setting the normal components of the external pressure tensor equal to $P_{ii} = 0\ \varepsilon/\sigma^3$, where $i = \{x, y, z\}$.

The equilibration procedure of the crosslinked systems involved only the last NPT stage. All crosslink bonds were unbreakable. We regarded the systems as fully equilibrated after the autocorrelation function of the end-to-end vectors

$$\varphi_{\mathrm{ee}}(t) = \frac{\langle \boldsymbol{R}_{\mathrm{ee}}(t_0) \cdot \boldsymbol{R}_{\mathrm{ee}}(t_0 + t) \rangle - \langle \boldsymbol{R}_{\mathrm{ee}} \rangle^2}{\langle \boldsymbol{R}_{\mathrm{ee}}^2 \rangle - \langle \boldsymbol{R}_{\mathrm{ee}} \rangle^2} \tag{4}$$

had decayed to zero [37], where $\boldsymbol{R}_{\mathrm{ee}}$ is the end-to-end vector of a chain. In practice, we allowed the systems to equilibrate for longer times than the relaxation time of φ_{ee}, to ensure thorough equilibration of the configurations.

RESULTS

Glass-Transition Temperature

We allowed the systems to relax at T = 0.8 $\varepsilon/k_{\mathrm{B}}$ and P = 0.0 ε/σ^3, until φ_{ee} had decayed to zero. We then performed NPT simulations for the calculation of the glass-transition temperature by lowering the temperature of the system with a cooling rate of $2 \cdot 10^{-5}$ $(\varepsilon/k_{\mathrm{B}})/\tau$ 0.02 $\varepsilon/k_{\mathrm{B}}$ per 10^3 τ in a stepwise fashion from 0.8 to 0.1 $\varepsilon/k_{\mathrm{B}}$. The glass-transition temperature was determined from a change in the slope above and below the transition region [7]. Evidently (Fig. 2) the slope-change within the transition region, i.e., the difference in the thermal expansivity below and above the T_{g}, is larger in the films than in the bulk.

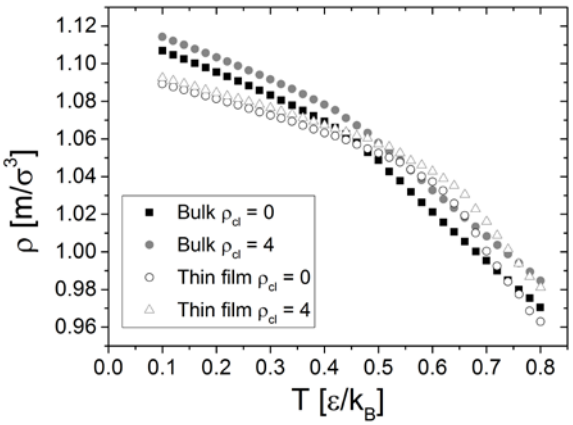

FIG 2: Density – temperature dependence for the bulk and the ultrathin film. Two different crosslinking densities (ρ_{cl}) are displayed. The average pressure was held constant and equal to zero for all systems.

This difference is also apparent in Fig 3, in which the thermal expansion coefficient is shown for temperatures above and below the glass-transition temperature. The thermal expansion coefficient (CTE) is defined as

$$\alpha_T = \frac{1}{\rho_0}\left(\frac{d\rho}{dT}\right)_P \tag{5}$$

where ρ_0 is the initial mass density of the polymer. Fig. 3 shows that the CTE of the films in the rubbery state is weakly dependent on confinement for the two thickest films, while it is slightly smaller in the ultrathin film. This could indicate that confinement affects the CTE only when the average film thickness approaches the bulk radius of gyration of the chains. In the glassy state, the CTE decreases when the polymer is confined and, though it is independent on the degree of confinement for the thick and thin films, it displays a strong decrease in the ultrathin film case where the film thickness is very close to the radius of gyration of the bulk.

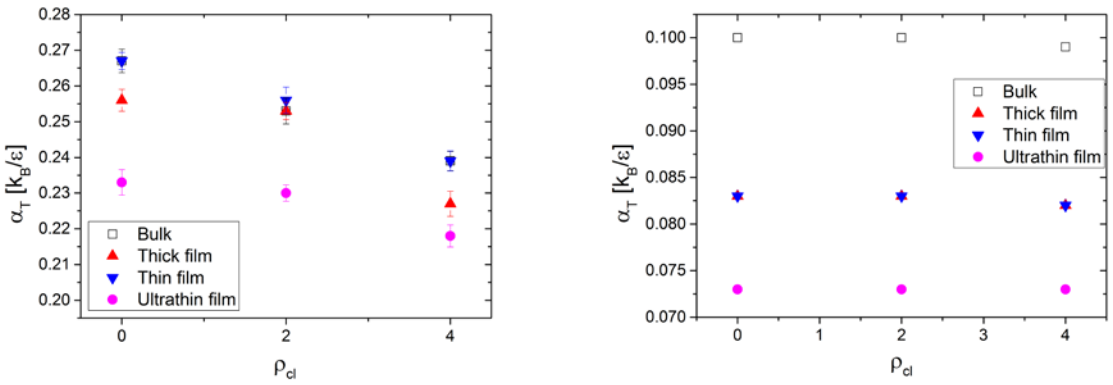

FIG 3: Thermal expansion coefficients as a function of the polymer crosslinking density (see Eq. 3). Left: Above T_g (rubber). Right: Below T_g (glass).

Apparently, crosslinks inhibit volume expansion in response to temperature increases, for $T > T_g$. We attribute this decrease in CTE to the decreased chain flexibility in systems with a larger number of crosslinks. As can be seen in Fig. 3, the calculated CTE above the T_g decreases with an increase in the overall crosslinking density, while it remains almost constant for temperatures lower than the T_g. The low values of CTE below the T_g are due to a higher polymer density and to a reduced molecular mobility, which decreases the volumetric response of the material to temperature changes.

The dependence of the glass-transition temperature on the crosslinking density and confinement is displayed in Fig. 4. It is evident that T_g is weakly affected by the crosslinking density, increasing linearly with increasing ρ_{cl}, while it is strongly affected by confinement: a higher degree of confinement results in a higher glass-transition temperature. The results qualitatively agree well with previous studies on capped polymer films that employed the same ratio of polymer-polymer and polymer-substrate interaction strength [12].

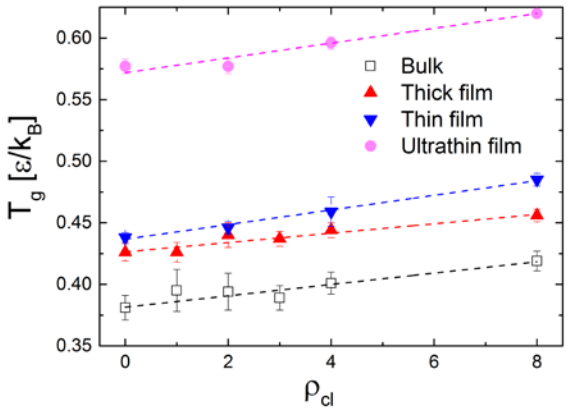

FIG 4: Glass-transition temperature as a function of crosslinking density and film thickness. The average pressure is constant and equal to zero for all systems.

A broader glass transition is often reported in nanocomposites than in the neat polymer matrix [6]. To elucidate on this observation we plotted the temperature dependence of the CTE (Fig. 5). Apparently, no clear distinction can be observed between the bulk and confined polymer in regards to the width of the glass transition region.

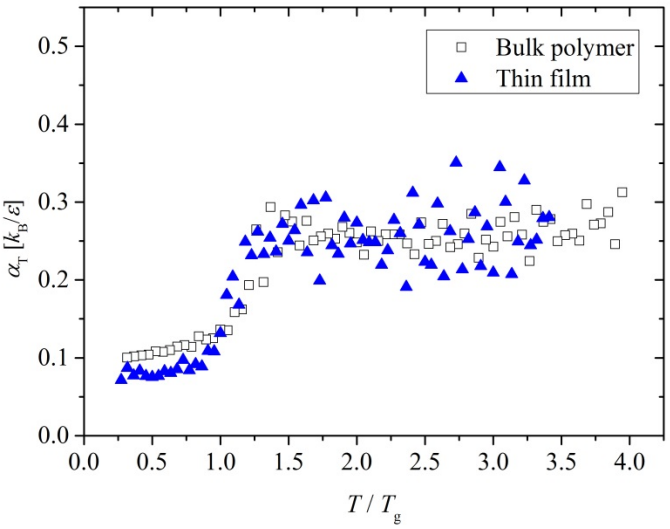

Fig 5: The temperature dependence of the thermal expansion coefficient for the bulk polymer and the thin film. The temperature axis is rescaled by dividing with the glass-transition

temperature of each system. No difference in the glass transition region is apparently observed between the bulk and the films.

Local Structure and Density

The spatial density profiles of the crosslinked and non-crosslinked systems in the direction perpendicular to the substrates are similar, which means that the crosslinking method we adopted did not affect the conformation of the chains. The density profiles are shown in Fig. 6, where we plot the mass density of the polymer as a function of the distance from the substrate.

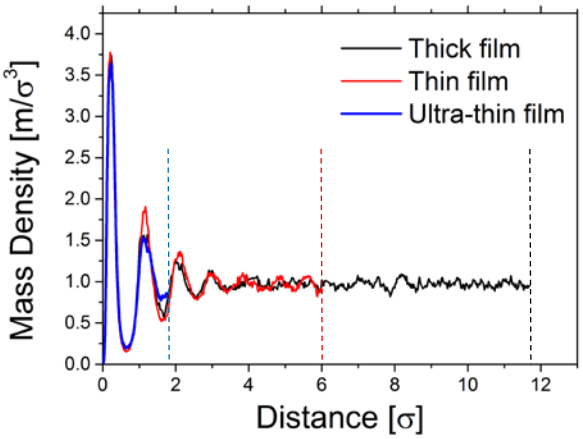

FIG 6: Spatial mass density profile of the monomer segments for the three films at T = 0.8 ε/k_B. In all films, the density oscillates around the bulk average value. Since the profiles are symmetric with respect to the middle of the film, only half of the film thickness is shown. The vertical dashed lines indicate the middle of each film along the direction perpendicular to the substrates.

Confining the polymer between two crystalline substrates creates layers of different densities whose relative size is independent of the degree of confinement. The polymer density displays its maximum value near the substrates, and it decreases towards the middle

of the film where it becomes equal to the density of the bulk. This is in agreement with similar simulation results found in the literature [7]. The density layers became more homogeneous as we increased the temperature (not shown).

Despite the strong structuration in the direction perpendicular to the substrates, neither confinement nor crosslinking perturbs the lateral structure of the polymer [19]. As shown in Fig. 7, the overall static structure factor displays a sequence of peaks whose amplitude rapidly decreases toward unity. This is an indication of the short-range order of the monomers, typically observed in amorphous materials.

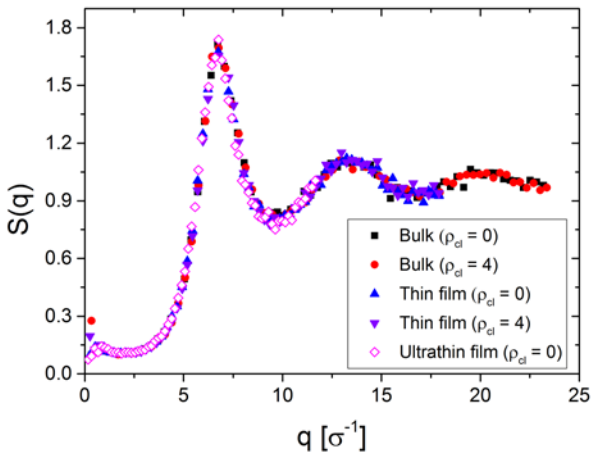

FIG 7: Overall static structure factor for various systems, at T = 1.2 ε/k_B. For the film data, we have used wave-vectors **q** parallel to the substrates.

The location of the first sharp diffraction peak is found approximately at q = 7.0 σ^{-1}. The overall static structure factor of the crosslinked systems displays a local maximum at low magnitudes of the wavevector $\boldsymbol{q}$, indicative of correlations at large scales. This correlation length is probably associated with the average distance between the crosslink junctions.

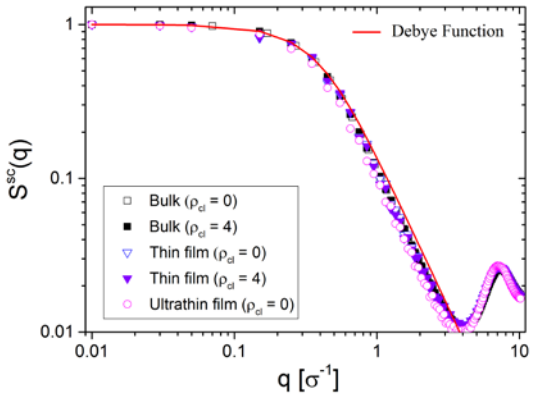

FIG 8: Form factor for various systems, at T = 1.2 ε/k_B. For the film data, we have used wave-vectors **q** parallel to the substrates. The slope in the scaling regime was calculated equal to -2 and -1.9 for the bulk and films, respectively, which indicates that the chains adopt random coil conformations. The Debye function is also plotted (Eq. 7).

In Fig. 8, we compare the form factor for systems with different crosslinking density and degree of confinement:

$$S^{\mathrm{sc}}(q) = \frac{1}{N_c}\left\langle \sum_{j=1}^{N_{mc}} \sum_{\mathrm{k}=1}^{N_{mc}} \exp\{i\boldsymbol{q}\cdot(\boldsymbol{R}_j^c - \boldsymbol{R}_{\mathrm{k}}^c)\} \right\rangle \tag{6}$$

where N_{c} is the number of polymer chains, N_{mc} is the number of monomers per chain, and $\boldsymbol{R}_j^c$ is the position of the j^{th} monomer of the c^{th} chain. The solid line within the figure represents the Debye formula for Gaussian coils [26]

$$S_{\mathrm{Debye}}^{\mathrm{sc}}(t) = \frac{2\,N_{\mathrm{mc}}}{(qR_{\mathrm{g}})^4}\left\{\exp\left[-(qR_{\mathrm{g}})^2\right] + (qR_{\mathrm{g}})^2 - 1\right\} \tag{7}$$

where the radius of gyration of the chains, R_g, was calculated from the simulations. It is evident that the form factor in all of the systems agrees well with the Debye function. This implies a Gaussian conformation on all length scales, from the collision diameter of adjacent monomers, along the backbone of the chain.

CONCLUSIONS

We employed a coarse-grained copolymer model to study the thermal-volumetric and structural properties of capped polymer films. We calculated the dependence of the mentioned properties on the polymer crosslinking density and the degree of confinement (film thickness) using molecular-dynamics simulations. We characterized the thermal and volumetric properties by computing the density, the thermal expansion coefficient, as well as the glass-transition temperature. Our simulation model, being of a coarse-grained nature, aims to the elucidation of generalized properties of polymer films rather than to the explanation of those kinds of properties that depend on chemical specifics; the latter are lost in our simulations. Therefore, a probable disagreement with experimental results, or with results of atomistic simulations, might serve as an indication of the importance of chemistry-dependent phenomena in observed behavior of the T_g.

We computed the structural properties of the mentioned systems by calculating the overall static structure factor of the monomers and the form factor of the chains. We saw that confinement does not influence the equilibrium structure of the polymer along the direction parallel to the substrates. In this direction, the chains adopt Gaussian conformations and the structure resembles an amorphous liquid. Confining the polymer though, induces the development of density layers along the perpendicular direction.

We found that the glass-transition temperature increases linearly with an increase in the crosslinking density, while it exhibits a stronger dependence on the degree of confinement

(increasing with a decreasing film thickness). Previously reported MD simulations of capped polymer films attribute the increasing T_g to the slow relaxation of monomers that lie close to the crystalline substrates, in comparison to the faster and bulk-like relaxation in the middle layers of the film. These slowly relaxing layers gradually enclose a larger volume fraction of the film as the film thickness is further decreased, and this is the attributed reason for the increasing T_g under stronger confinement. We expect the presence of crosslink bonds to further inhibit the structural relaxation of the polymer and therefore the crosslinking density to have a similar to the film thickness effect on the T_g. This is apparently true in our study; but to affirm this assumption, a study of the structural relaxation in films of different thickness and crosslinking density should be performed; and this is planned for a future publication.

ACKNOWLEDGMENTS

This work is a part of FOM research project #11VEC06. It was also sponsored by the Stichting Nationale Computerfaciliteiten (National Computer Facilities Foundation, NCF) for the use of supercomputer facilities, with financial support from the Nederlandse Organisatie voor Wetenschappelijk Onderzoek (Netherlands Organization from Scientific Research, NWO). We would like to thank Prof. Daniel Bonn (University of Amsterdam, experimental part of the project), Dr. Christos Tzoumanekas (National Technical University of Athens), Prof. Thijs Michels (Eindhoven Univerisyt of Technology), as well as the industrial partners SKF and Michelin for their helpful discussions.

REFERENCES

1. G. Allegra, G. Raos, and M. Vacatello, *Prog. Polym. Sci.*, **33**, 7 (2008).

2. P. Rittigstein, R. D. Priestley, L. J. Broadbelt, and J. M. Torkelson, *Nat. Mater.*, **6** (2007).

3. A. Bansal, H. Yang, C. Li, K. Cho, B. C. Benicewicz, S. K. Kumar, and L. S. Schadler, *Nat. Mater.*, **4** (2005).

4. S. Sen, Y. Xie, A. Bansal, H. Yang, K. Cho, L. S. Schadler, and S. K. Kumar, *Eur. Phys. J. Special Topics*, **141**, 161-165 (2007).

5. J. M. Kropka, V. Pryamitsyn, and V. Ganesan, *Phys. Rev. Lett.*, **101**, 075702 (2008).

6. K. S. Khare and R. Khare, *J. Phys. Chem. B*, **117**, 7444 (2013).

7. C. Batistakis, A. V. Lyulin, and M. A. J. Michels, *Macromolecules*, **45**, 17 (2012).

8. C. Batistakis, M. A. J. Michels, and A. V. Lyulin, *AIP Conf. Proc.*, **1599**, 62 (2014).

9. C. Batistakis, M. A. J. Michels, and A. V. Lyulin, *J. Chem. Phys.*, **139**, 024906 (2013).

10. D. V. Guseva, P. V. Komarov, and A. V. Lyulin, *J. Chem. Phys.*, **140**, 114903 (2014).

11. D. Hudzinskyy, A. V. Lyulin, A. R. C. Baljon, N. K. Balabaev, and M. A. J. Michels, *Macromolecules*, **44**, 7 (2011).

12. A. C. Batistakis, A. V. Lyulin, and M. A. J. Michels, *Macromolecules*, **47** (2014).

13. M. Solar, E.U. Marpesa, F. Kremer, K. Binder, and W. Paul, *EPL*, **104**, 66004 (2013).

14. F. Varnik, J. Baschnagel, and K. Binder, *Phys. Rev. E*, **65**, 021507 (2002).

15. F. Varnik, *Eur. Phys. J. E*, **8**, 175 (2002).

16. J. A. Torres, P. F. Nealey, and J. J. De Pablo, *Phys. Rev. Lett.*, **85**, 3221 (2000).

17. G. D. Smith, D. Bedrov, and O. Borodin, *Phys. Rev. Lett.*, **90**, 226103 (2003).

18. S. Peter, S. Napolitano, H. Meyer, M. Wubbenhorst, and J. Baschnagel, *Macromolecules*, **41**, 7729 (2008).

19. J. Liu, D. Cao, and L. Zhang, *J. Chem. Phys.*, **131**, 034903 (2009).

20. N.J. Soni, PH Lin, and R. Khare, *Polymer*, **53**, 4 (2012).

21. T. W. Sirka, K. S. Khareb, M. Karimb, J. L. Lenharta, J. W. Andzelma, G. B. McKennab, and R. Khare, *Polymer*, **54**, 26 (2013).

22. A. Shokuhfar and B. Arab, *J. Mol. Model.*, **19**, 9 (2013).

23. J. Liu, D. Cao, and L. Zhang., *J. Chem. Phys*., **131**, 034903 (2009).

24. J.L. Keddie, R.A.L Jones, and R.A Cory, *Faraday Discuss*., **98** (1994).

25. J.A. Forrest, K. Dalnoki-Veress, J.R. Stevens, and J.R. Dutcher, *Phys. Rev. Lett*., **77** (1996).

26. T. Kanaya, T. Miyazaki, R. Inoue, and K. Nishida, *Physica Status Solidi (b)*, **242** (2005).

27. G.B. DeMaggio, W.E. Frieze, D.W. Gidley, M. Zhu, H.A. Hristov, and A.F. Yee, *Phys. Rev. Lett.*, **78** (1997).

28. G. Heinrich, M. Kluppel, *Adv. Polym. Sci.*, **160** (2002).

29. G. Heinrich, M. Kluppel, and T.A. Vilgis, *Curr. Opin. Solid State Mater. Sci*., **6** (2002).

30. M. Kluppel, *Adv. Polym. Sci*., **164** (2003).

31. M. Kluppel, G. Heinrich, *Kautsch. Gummi Kunstst*., **58** (2005).

32. M. Tress, M. Erber, E. U. Mapesa, H. Huth, J. Müller, A. Serghei, C. Schick, KJ. Eichhorn, B. Voit, and F. Kremer, *Macromolecules*, **43**, 23 (2010).

33. J. L. Keddie and R. A. L. Jones, Europhys. Lett. 27, 59 (1994).

34. V. Lupa¸scu, S. J. Picken, and M. J. Wubbenhorst, Non-Cryst. Solids 352, 5594 (2006).

35. S. Kawana and R. A. L. Jones, Phys. Rev. E 63, 021501 (2001).

36. K. W. Putz, M. J. Palmeri, R. B. Cohn, R. Andrews, and L.C. Brinson, *Macromolecules*, **41**, 6752 (2008).

37. S. Plimpton, *J. Comp. Phys.*, **117**, 1 (1995).

38. K. Kremer and G. S. Grest, *J. Chem. Phys.*, **92**, 5057 (1990).

39. C. Tzoumanekas, F. Lahmar, B. Rousseau, and D. N. Theodorou, *Macromolecules*, **42**, 19 (2009).

40. W. Humphrey, A. Dalke, and K. J. Schulten, *J. Mol. Graphics*, **14**, 1 (1996).

41. C. Batistakis and A.V. Lyulin, *Comp. Phys. Comm.*, **185**, 4 (2014).

42. W. Kob and H. C. Andersen, *Phys. Rev. Lett.*, **73**, 1376 (1994).

43. W. Kob and H. C. Andersen, *Phys. Rev. E*, **51**, 4626 (1995).

44. M. Aichele and J. Baschnagel, *Eur. Phys. J. E*, **5**, 2 (2001).

45. T. Mulder, *Equilibration and deformation of glass-forming polymers : molecular simulation via connectivity-altering Monte Carlo and scale-jumping methods*, PhD Thesis, Technische Universiteit Eindhoven (2008).

46. M. Doi and S. F. Edwards, *The Theory of Polymer Dynamics*, Oxford University Press (1990).